ISBN: 978-628-96613-3-0. ISSN: 2414-6390. Digital Object Identifier: https://dx.doi.org/10.18687/LACCEI2026.1.1.2462

Multiobjective Torque Ripple Minimization of a BLDC Motor Using NSGA-II

José D. Gadea-Vázquez[1]; Carlos A. Jiménez-Carballo[2]
[1,3] *Costa Rica Institute of Technology, Cartago, Costa Rica, joseda18@estudiantec.cr, carjimenez@itcr.ac.cr*

***Abstract*– Torque stability in ventricular assist devices (VADs) is critical to maintaining continuous blood flow and reducing adverse hemodynamic effects. This work presents a multi-objective geometric optimization of a brushless DC (BLDC) motor with an axial, shaftless design for VAD applications. A two-dimensional finite element model in COMSOL Multiphysics was coupled with MATLAB via LiveLink™ to evaluate candidate geometries. Five rotor and stator parameters were selected as design variables, and three objectives were defined: minimizing torque variation, enforcing a minimum average torque of 50 mN·m, and regulating the air-gap area. Optimization was performed using the NSGA-II algorithm with approximately 5000 evaluations. Results reduced torque ripple from 14.8% in the baseline design to below 5% within the Pareto set while satisfying the torque constraint. A trade-off between ripple reduction and average torque was observed. The proposed framework proves to be an effective tool for the electromagnetic optimization of BLDC motors in biomedical applications.**

***Keywords*-- BLDC motor, ventricular assist device, ripple torque, evolutionary algorithms, NSGA-II.**

I. Introduction

Currently, a Ventricular Assist Device (VAD) is being developed at the Costa Rica Institute of Technology (TEC). This device employs an axial impeller without a central shaft, aiming to minimize the impacts on people's blood by reducing mechanical contact and wear, thereby optimizing the efficiency and durability of the device [1]. A brushless direct current (BLDC) motor is proposed as the actuation system for the device [2]. This choice is because BLDC motors have been recognized as one of the most suitable technologies for biomedical applications, as they offer several advantages compared to brushed DC and induction motors. For instance, they exhibit higher efficiency due to reduced mechanical friction losses, their speed is determined by the supply current frequency rather than voltage, which further enhances efficiency, they can operate at high speeds under varying conditions, generate lower acoustic noise during operation, and present an improved torque–speed relationship, making them particularly suitable for such applications [3], [4].

Despite their advantages, BLDC motors inherently exhibit ripple torque, characterized by periodic variations in electromagnetic torque during operation. These oscillations produce mechanical vibrations, which can contribute to increased wear, decreased efficiency, and poor speed regulation [5]. In biomedical applications such as VADs, torque ripple can cause differences in blood flow, significantly impacting the patient's hemodynamics. A continuous and smooth blood flow is required to protect blood cells and guarantee proper organ perfusion. [6], [7].

Preliminary simulations of an axial VAD with a shaftless impeller being developed as part of a broader research effort at the Costa Rica Institute of Technology found a high torque ripple of 14.8% relative to the average torque, indicating the need for geometric optimization of the motor design [2]. Traditional control-based mitigation solutions, such as field-oriented control, may reduce ripple; however, structural geometric optimization provides a supplementary approach by directly changing the magnetic interaction between stator and rotor components [8].

When investigated with finite element simulations, the relationship between internal geometric parameters and torque production in BLDC motors is highly nonlinear and not analytically differentiable [9]. The model implemented in COMSOL Multiphysics constitutes a black-box optimization problem, where each evaluation requires a full electromagnetic simulation. Additionally, the existence of numerous local optima necessitates the employment of stochastic global optimization techniques instead of gradient-based approaches [10].

Therefore, this work aims to develop a solution that minimizes the ripple torque of a brushless direct current (BLDC) motor by modifying its geometric properties using a multi-objective evolutionary approach based on the NSGA-II genetic algorithm. First, five key geometric parameters of the motor's rotor and stator are selected as decision variables, and their influence is evaluated using coupled MATLAB-COMSOL simulations. Subsequently, the NSGA-II evolutionary algorithm is implemented to obtain a set of optimal values that minimize the ripple torque in the BLDC motor. Finally, the set of optimized candidate designs is analyzed to determine the best candidate based on the motor's operating requirements.

I. Methodology

A. Electromagnetic FEM Model

The electromagnetic behaviour of the BLDC motor was evaluated using a two-dimensional FEM model implemented in COMSOL Multiphysics, based on the original .mph file used in [2]. This file established fixed boundaries, including the number of poles, slots, external diameter, and physical study settings for torque ripple. All of these were preserved without modification in accordance with design constraints defined in the underlying research [2]. A cross-section of the motor is shown in Fig. 1.

Torque was computed using the Arkkio method, which evaluates electromagnetic torque from the Maxwell stress tensor integrated over the air-gap region. In addition, physical studies unrelated to cogging torque were eliminated, and the maximum simulation time was reduced to one quarter of the original value, ensuring that each simulation completed at least two periods of cogging torque.

B. Design Variable Selection

The geometric design variables considered for optimization were identified through a review of the existing literature and preliminary parametric simulations.

Parameters exhibiting significant influence on torque ripple were selected as decision variables, along with the internal constraints of the 2D FEM model, avoiding linear constraints and dependencies, to be able to define clear limits of variation for run efficiency. Fig. 2 illustrates the geometric definition of these variables, while Table I summarizes their corresponding construction limits.

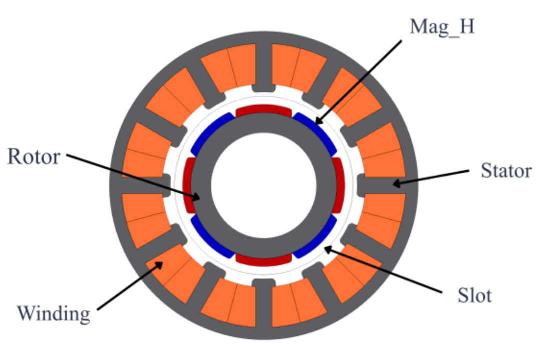

Fig 1. Two-dimensional FEM model of the BLDC motor.

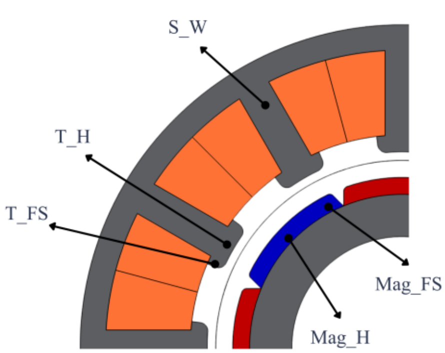

Fig. 2. Geometric design variables considered in the multiobjective optimization.

TABLE I
LIMITS DEFINED FOR THE GEOMETRIC PARAMETERS OF THE BLDC MOTOR.

Parameter	Description	Location	Limits (mm)
Mag_H	Magnet height	Inner rotor	1.0 – 3.0
Mag_FS	Magnet fillet radius	Inner rotor	0.1 – 1.4
S_W	Tooth shoe width	Stator	3.0 – 6.0
T_H	Stator tooth height	Stator	3.0 – 6.0
S_FS	Shoe fillet radius	Stator	0.1 – 1.0

C. Objective Function Definition

The optimization problem was formulated in (x) as a three-objective minimization problem

$$\min_{x\in\Omega} \boldsymbol{f}(\boldsymbol{x}) = [f_1(x), f_2(x), f_3(x)], \quad (1)$$

Where $x \in \mathbb{R}^m$ represents the vector of geometric design variables, and Ω denotes the feasible design space defined by the bounds of these variables as specified in Table I. The objective functions are minimized simultaneously in the Pareto sense, yielding a set of non-dominated solutions. Specifically, each of the functions are defined as:

$$f_1(x) = \mathrm{T}_{\max} - \mathrm{T}_{\min}, \quad (2)$$

$$f_2(x) = \begin{cases} 0, & T_{avg} \geq 50 \\ 50 - T_{avg}, & T_{avg} < 50, \end{cases} \quad (3)$$

$$f_3(x) = g(x). \quad (4)$$

Here, $\mathrm{T}_{\max}$ and $\mathrm{T}_{\min}$ denote the maximum and minimum torque values within one electrical period, $\mathrm{T}_{\mathrm{avg}}$ is the corresponding average torque, and g represents the air-gap area between the stator and rotor. The second objective enforces the minimum torque requirement of 50 mN·m through a penalty function.

The torque ripple is usually defined as the difference between the maximum and minimum torque in a revolution expressed as a percentage value, that is:

$$T_{ripple} = \frac{T_{max} - T_{min}}{T_{avg}} \cdot 100. \quad (5)$$

This definition has been used to select the optimized results. Finally, $f_1(x)$ has been defined as a simplified form of (5) to reduce computation time in the algorithm's implementation.

D. Multiobjective Genetic Algorithm

The multiobjective optimization was performed using MATLAB's gamultiobj function, which implements a controlled elitist genetic algorithm based on the principles of the Non-Dominated Sorting Genetic Algorithm II (NSGA-II) [11]. Candidate solutions were ranked using nondominated sorting, while diversity along the Pareto front was maintained through a crowding distance metric.

The algorithm was configured with a population size of 50 individuals and a maximum of 100 generations, corresponding to approximately 5000 objective function evaluations. Scattered crossover was employed with a crossover fraction of 0.6, and mutation was performed using the mutationadaptfeasible operator. These parameter values are consistent with common practice in multiobjective evolutionary optimization [11].

Bound constraints on the design variables were directly enforced by the solver. The minimum average torque requirement was incorporated as a soft constraint through the penalty-based objective formulation described in Section 2.B, thereby penalizing solutions that violated the prescribed torque threshold while preserving them within the search space.

E. Coupled COMSOL-Matlab Implementation

The electromagnetic finite-element model and the genetic algorithm were coupled through LiveLink™ for MATLAB, which provides a bidirectional interface between COMSOL Multiphysics and MATLAB via the COMSOL API, as illustrated in Fig. 3.

The geometry and corresponding mesh were updated programmatically in MATLAB prior to each simulation. The mesh curvature factor was set from 0.3 to 0.8 to control element density, resulting in simulation times of approximately 15-20 s per design.

For each updated geometry, a transient electromagnetic simulation was executed in COMSOL through LiveLink™, and torque time-series data were extracted back into MATLAB for objective evaluation. Average torque and maximum/minimum torque were computed in MATLAB from the returned solution fields to evaluate the multiobjective fitness functions defined in Section 1.C. The optimization loop continued automatically, computing objectives until the stopping criteria were met. This computational framework enables a systematic exploration of the motor design space by integrating FEM-based electromagnetic evaluation with evolutionary optimization. As a result, it allows the identification of non-dominated solutions under multiple competing objectives, without requiring analytical gradients or simplified models.

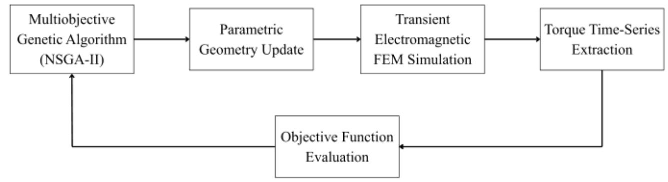

Fig. 3. Computational workflow of the coupled COMSOL–MATLAB multiobjective optimization framework.

III. RESULTS AND DISCUSSION

This section shows the solutions provided by Pareto Front from the genetic algorithm and the selection by comparison for best solutions.

F. Multiobjective Genetic Algorithm Results

The GA (Genetic Algorithm) resulted in a Pareto Front of 36 possible geometry configurations, in which the Fig. 4 shows the three objectives of optimization. The optimal selected solutions were marked in orange, those satisfy the minimum threshold requirement of 50 mN·m. The trade-off between objectives is clearly visible in the three-dimensional space. Designs that meet the threshold constraint tend to exhibit larger air-gap integral values, which are associated with increased torque variation. This indicates that satisfying the threshold requirement imposes a cost in terms of air-gap integral and torque ripple performance.

Conversely, solutions that achieve very low torque variation are primarily found in regions where the threshold constraint is violated and larger air-gap integrals are permitted. The concentration of points near zero in the torque variation axis highlights this behavior.

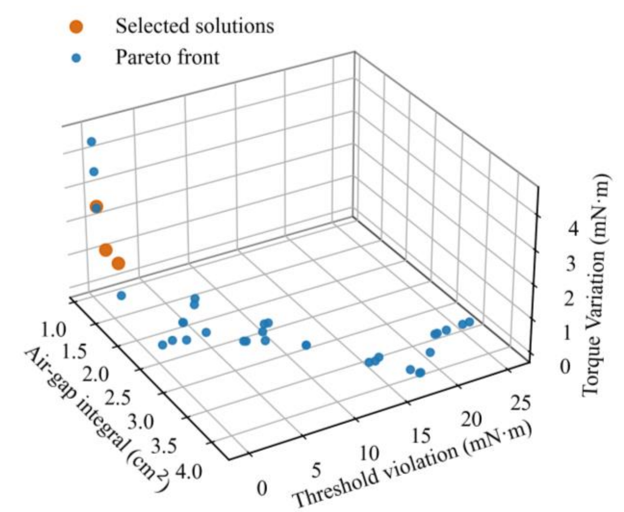

Fig. 4 Three-Dimensional Pareto Front.

The evolution of the Pareto distance across generations is shown in Fig. 5. A clear decreasing trend is observed from approximately generation 8 to generation 42, indicating progressive refinement of the Pareto front approximation. A brief stabilization occurs between generations 38 and 42, suggesting that the algorithm reached a near-steady solution set during this stage.

A spike is observed around generation 45. This behavior is attributed to penalized individuals introduced when COMSOL simulations failed, temporarily perturbing the non-dominated set. Despite this fluctuation, the overall downward trend and subsequent recovery indicate that the algorithm maintained a general convergence trend.

The Pareto spread evolution is presented in Fig. 6. The spread metric reflects the distribution and diversity of solutions along the Pareto front. While a mild decreasing tendency is observed, the metric does not collapse toward zero, indicating that the population did not suffer from premature convergence.

A temporary increase around generation 45 is again associated with penalized individuals resulting from occasional simulation failures. Importantly, the spread stabilizes in later generations at a non-zero value, demonstrating that solution diversity was preserved while convergence progressed. This balance between stabilization of the Pareto distance and maintenance of spread confirms that the algorithm achieved a well-distributed and stable approximation of the Pareto front.

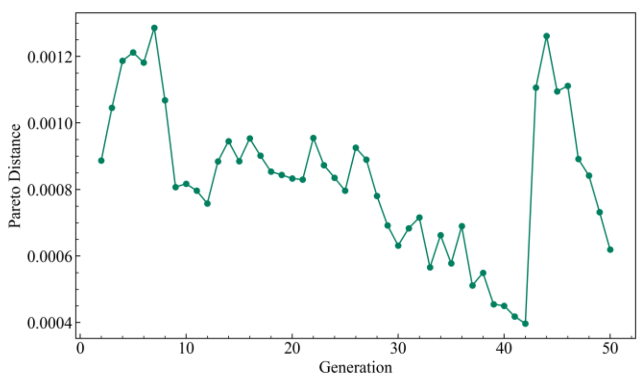

Fig. 5 Generation vs Pareto Distance

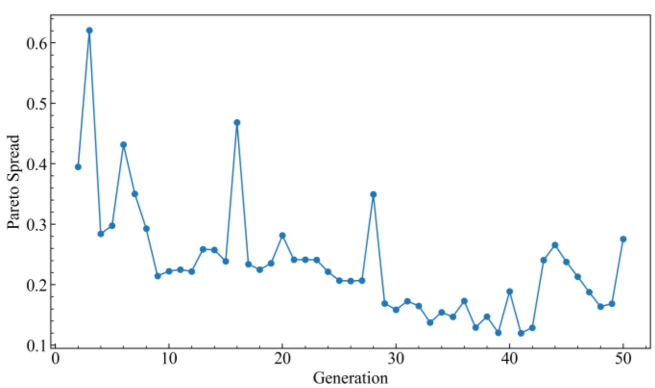

Fig. 6 Generation vs Pareto Spread

G. Selected Pareto-Optimal Designs and Performance Comparison

From the non-threshold-violating solutions shown in Table II, three representative configurations (A, C, and F) were selected for detailed analysis. These designs were chosen in ascending order from the minimum torque ripple results.

As shown in Table II, configuration A achieves an axial torque of 58.02 mN·m and the lowest torque ripple of the group of 2.71%. Configuration F exhibits a nearly identical ripple value of 2.77% but produces a lower axial torque of 54.08 mN·m. Configuration C, on the other hand, increases axial torque to 61.75 mN·m, though at the cost of a higher ripple of 4.25%.

This indicates that reducing ripple tends to limit achievable axial torque within the explored design space. Configuration E demonstrates that higher torque can be achieved, but ripple increases accordingly. The air-gap integral also reflects this trade-off, as lower air-gap values tend to produce higher average axial torque, as shown in Configurations C and D. Although, high axial torque values can be achieved with higher air-gap values with a compromised higher torque ripple as shown in Configuration E.

Table III presents the geometric parameters of the selected designs compared to the original configuration and Fig. 7 provides a visual comparison of these geometries. A clear deviation from the original geometry is observed in all optimized designs. The magnet height (Mag_H) increases slightly in all selected configurations (from 1.00 mm to approximately 1.04–1.07 mm), indicating that a modest increase in magnet thickness contributes positively to performance.

The most significant change appears in the magnet fillet radius (Mag_FS), which increases substantially from 0.30 mm in the original design to values between 1.24 mm and 1.35 mm

TABLE II
COMPARATIVE OUTCOMES OF THE MOST OPTIMAL CONFIGURATIONS

Index	Axial torque (mN*m)	Torque Ripple (%)	Air-gap integral (cm^2)
Original	95.4	14.8	14.72
A	58.02	2.71	1.35
B	58.71	8.94	1.68
C	61.75	4.25	1.16
D	63.42	5.71	1.14
E	64.39	6.93	1.99
F	54.08	2.77	1.62

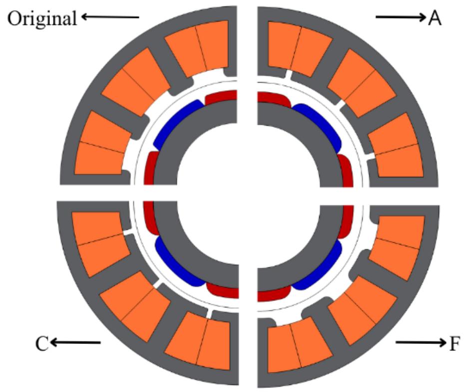

Fig. 7 Candidate Geometry Comparison

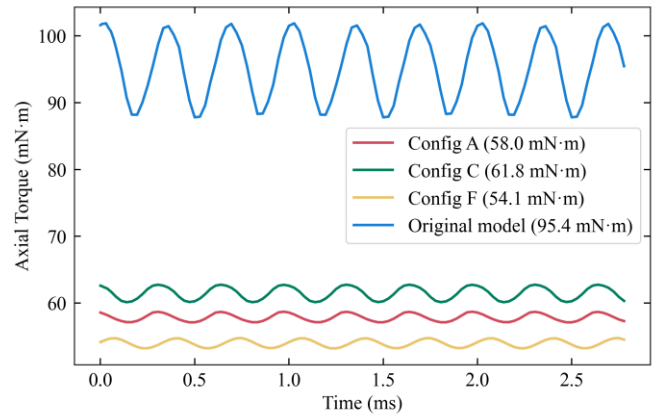

Fig. 8 Time-Domain Torque Comparison of Original and Optimized Configurations

TABLE III
VALUES OF GEOMETRIC PARAMETERS FOR THE MOST OPTIMAL CONFIGURATIONS

Config.	Mag_H (mm)	Mag_FS (mm)	S_W (mm)	T_H (mm)	S_FS (mm)
Original	1.00	0.30	3.00	6.00	0.50
A	1.07	1.35	5.94	5.75	0.15
C	1.04	1.29	5.94	5.98	0.15
F	1.07	1.24	3.81	5.75	0.80

in the optimized solutions. This suggests that expanding the effective magnet span plays a major role in reducing torque ripple.

Tooth shoe width (S_W) exhibits the same tendency to increase in all configurations. Configurations A and C nearly double the slot width (5.94 mm compared to 3.00 mm in the original design), while configuration F maintains a more moderate increase (3.81 mm).

Tooth height (T_H) remains relatively stable across all configurations, with slight reductions from 6.00 mm to approximately 5.75–5.98 mm. This suggests that the original length provided by the motor was very close to a local optimum for the objective optimization.

The slot fillet size (S_FS) presents the most contrasting variation. While configurations A and C significantly reduce this parameter (0.15 mm), configuration F increases it to 0.80 mm compared to 0.50 mm in the original design. This geometric difference between the configurations likely suggests that S_FS may not affect significatively the results.

The Fig. 8 showcases the axial torque comparison between the original configuration and the three selected solutions, in which all three solutions reduced the torque ripple significantly, at the cost of a lower axial torque. The baseline configuration of the motor exhibited a torque ripple of 14.8%, which can be interpreted as a significant source of flow variability. In rotary blood pumps, hemolysis has been strongly correlated with both shear stress magnitude and exposure time, as described by empirical power-law models such as those proposed by Heuser and Opitz [12]. Configuration A managed to reduce the torque ripple by a factor of 5.46, while Config C and Config F resulted in a reduction factor of 3.48 and 5.34 respectively. In terms of torque ripple reduction, configuration A and F are ideal.

In contrast, the optimized configurations presented in this work reduced torque ripple to values below 5%, with the best candidates achieving approximately 2.7%. This reduction is expected to promote a more stable rotational regime, leading to smoother and more continuous blood flow. From a fluid dynamics standpoint, lower torque ripple minimizes temporal variations in angular velocity, thereby reducing secondary flow structures, intermittent high-shear events, and regions of flow separation within the pump. According to hemolysis models, reducing these fluctuations can significantly decrease cumulative blood damage, even if peak shear stresses remain unchanged.

H. Limitations

One of the main limitations of this study lies in the exclusively two-dimensional modeling approach, which does not aim to validate results in three dimensions. Nevertheless, the experimental validity of comparable 2D models has been previously demonstrated [13]. These studies suggest that the same methodological framework could be extended to a three-dimensional model to validate optimized designs.

However, torque evaluation is based on the Arkkio method applied within a two-dimensional FEM formulation. While this approach provides consistent and computationally efficient torque estimation, it does not capture three-dimensional effects such as axial flux variations, end effects, and fringing fields. As a result, the predicted torque values may differ from those of a fully three-dimensional axial motor configuration.

In addition, the development is constrained by the restrictions imposed by the original motor design and the guidelines of the associated research, which limit the range of modifiable parameters. Specifically, key features such as the number of poles, slots, external diameter, and physical study settings for torque ripple were fixed. Consequently, the optimized solutions are valid only within these design constraints.

A. Variability of the evolutionary algorithm

Due to the stochastic nature of the NSGA-II algorithm, variability in the optimization process is expected, as the initial population and genetic operators introduce randomness in the search trajectory. However, the observed convergence of the Pareto distance and the stabilization of the spread metric across generations indicate that the algorithm consistently evolves toward a stable and well-distributed set of solutions. Although only a single optimization run was performed, the smooth convergence behaviour and preservation of diversity suggest that the obtained Pareto front is representative of the underlying trade-offs of the problem.

III. Conclusions

This work led to the development of a multi-objective geometric optimization framework to minimize torque ripple in a BLDC motor intended for use in a ventricular assist device (VAD). This was achieved by combining a two-dimensional finite element electromagnetic model implemented in COMSOL Multiphysics with a multi-objective evolutionary algorithm (NSGA-II) executed in MATLAB.

This study demonstrates that torque ripple in BLDC motors for ventricular assist devices can be significantly reduced through targeted geometric modifications of the rotor–stator configuration. The optimized designs achieved ripple values below 5%, representing a substantial improvement compared to the baseline configuration (14.8%).

The results reveal a clear trade-off between torque smoothness and average torque production, highlighting the multi-objective nature of the electromagnetic design problem. In particular, parameters such as magnet fillet radius and stator slot width were identified as key contributors to ripple reduction, while other variables exhibited lower sensitivity within the explored design space.

From a biomedical perspective, reducing torque ripple is directly associated with improved flow stability inside the pump, which is a critical factor in minimizing hemolysis and ensuring consistent organ perfusion. Therefore, the obtained results suggest that electromagnetic optimization plays a relevant role not only in motor efficiency but also in the overall biocompatibility of the device.

Finally, these findings support the use of geometry-driven optimization as a complementary strategy to control-based approaches for improving the performance of BLDC motors in biomedical applications. Future work should focus on extending the analysis to three-dimensional models and coupling the electromagnetic results with fluid dynamic simulations to directly evaluate blood damage.

Acknowledgment

The authors gratefully acknowledge the support provided by the School of Physics and the Academic Doctoral Program in Engineering at the Costa Rica Institute of Technology during the development of this research. This publication derives from the research project entitled “Desarrollo de un sistema de mecánica auxiliar para un impulsor axial sin eje central” (Project Code: 5402-1450-2101), officially registered with the VIE at the Costa Rica Institute of Technology. This work was carried out by an undergraduate student in partial fulfillment of the requirements for the Bachelor’s Degree in Engineering Physics (Licenciatura en Ingeniería Física) at the Costa Rica Institute of Technology.

References

[1] G. Ortiz-León *et al.*, “Estudio exploratorio para el desarrollo de un dispositivo de asistencia cardiaca,” Cartago, 2012.

[2] C. A. Jiménez-Carballo and G. Ortiz-León, “Comparative study of four BLDC motor configurations for a ventricular assist device with axial impeller without central axis,” in *Proceedings of the LACCEI international Multi-conference for Engineering, Education and Technology*, 2025. doi: 10.18687/LACCEI2025.1.1.2038.

[3] C. L. Xia, *Permanent Magnet Brushless DC Motor Drives and Controls*. 2012. doi: 10.1002/9781118188347.

[4] A. Fenercioğlu, “Design and Analysis of Magnetically Levitated AxialFlux BLDC Motor For Ventricular Assist Device (VAD),” *Turkish Journal of Electrical Engineering and Computer Sciences*, vol. 24, May 2016, doi: 10.3906/elk-1405-139.

[5] M. S. Rafaq, W. Midgley, and T. Steffen, “A Review of the State of the Art of Torque Ripple Minimization Techniques for Permanent Magnet Synchronous Motors,” *IEEE Trans. Industr. Inform.*, vol. 20, no. 1, 2024, doi: 10.1109/TII.2023.3272689.

[6] M. S. Slaughter and R. Singh, “El papel de los dispositivos de asistencia ventricular en la insuficiencia cardiaca avanzada,” *Rev. Esp. Cardiol.*, vol. 65, no. 11, 2012, doi: 10.1016/j.recesp.2012.02.030.

[7] G. A. Giridharan, M. Skliar, D. B. Olsen, and G. M. Pantalos, “Modeling and control of a brushless DC axial flow ventricular assist device,” *ASAIO Journal*, vol. 48, no. 3, 2002, doi: 10.1097/00002480-200205000-00013.

[8] K. Abbaszadeh, F. R. Alam, and S. A. Saied, “Cogging torque optimization in surface-mounted permanent-magnet motors by using design of experiment,” *Energy Convers. Manag.*, vol. 52, no. 10, 2011, doi: 10.1016/j.enconman.2011.04.009.

[9] S. J. Salon, *Finite Element Analysis of Electrical Machines*. 1995.

[10] D. Griffel, “Multi-objective optimization using evolutionary algorithms,” *The Mathematical Gazette*, vol. 87, no. 509, 2003, doi: 10.1017/s0025557200173498.

[11] K. Deb, A. Pratap, S. Agarwal, and T. Meyarivan, “A fast and elitist multiobjective genetic algorithm: NSGA-II,” *IEEE Transactions on Evolutionary Computation*, vol. 6, no. 2, 2002, doi: 10.1109/4235.996017.

[12] G. Heuser and R. Opitz, “A Couette viscometer for short time shearing of blood,” *Biorheology*, vol. 17, no. 1–2, 1980, doi: 10.3233/bir-1980-171-205.

[13] M. Soyaslan, M. Bazazian, and O. Eldoğan, “Comprehensive Design and Testing of a BLDC Motor for Direct Drive EV Applications,” *Journal of Materials and Mechatronics: A*, vol. 6, no. 1, 2025, doi: 10.55546/jmm.1590391.